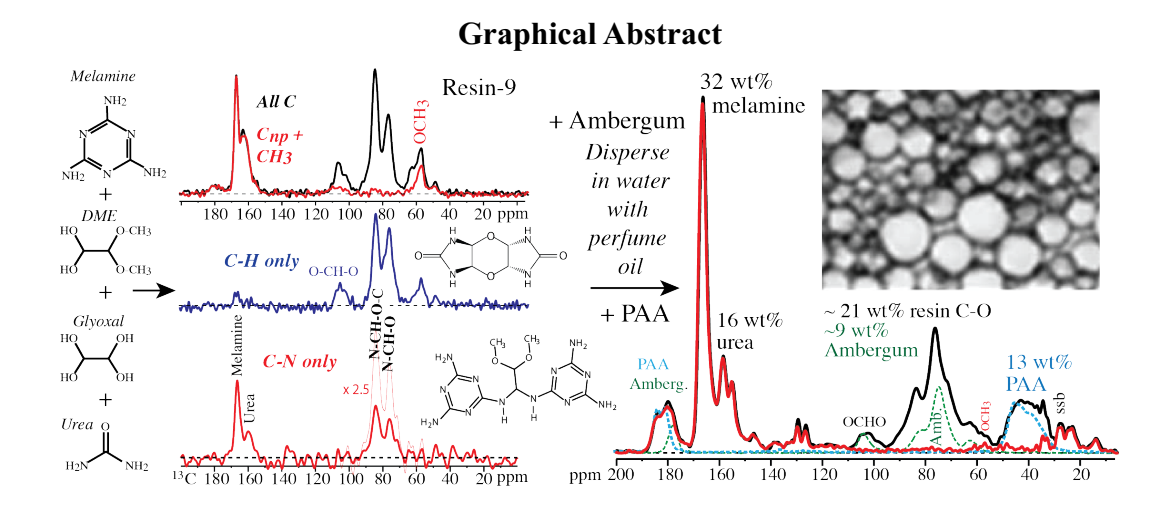
# Multinuclear Solid-State NMR of Complex Nitrogen-Rich Polymeric Microcapsules: Weight Fractions, Spectral Editing, Component Mixing, and Persistent Radicals

Shichen Yuan<sup>1</sup>, Pu Duan<sup>1</sup>, Damien L. Berthier<sup>2</sup>, Géraldine León<sup>2</sup>, Horst Sommer<sup>2</sup>, Jean-Yves de Saint-Laumer<sup>2</sup>, Klaus Schmidt-Rohr<sup>1\*</sup>

- 1: Department of Chemistry, Brandeis University, 415 South Street, Waltham, MA 02453, USA
- 2: Firmenich SA, Corporate Research Division, 1 Routes des Jeunes, 1211 Genève 8, Switzerland
- \* Corresponding author: srohr@brandeis.edu

# Submitted to Solid State NMR for the special issue on industrial applications of solid-state NMR $Revised\ Jan.\ 2020$



# **Highlights**

- The structure of a crosslinked N-rich resin was determined by multinuclear NMR.
- $-{}^{13}C$ ,  ${}^{13}C\{{}^{1}H\}$ ,  ${}^{1}H-{}^{13}C$ ,  ${}^{1}H$ ,  ${}^{13}C\{{}^{14}N\}$ , and  ${}^{15}N$  solid-state NMR methods were employed.
- Microcapsules made from the resin and other polymeric components were analyzed.
- The weight fractions of the microcapsule components were determined by NMR.
- NMR revealed crystallites in a resin and persistent radicals in microcapsules.

#### **Abstract**

The molecular structure of a crosslinked nitrogen-rich resin made from melamine, urea, and aldehydes, and of microcapsules made from the reactive resin with multiple polymeric components in aqueous dispersion, has been analyzed by <sup>13</sup>C, <sup>13</sup>C{<sup>1</sup>H}, <sup>1</sup>H-<sup>13</sup>C, <sup>1</sup>H, <sup>13</sup>C{<sup>14</sup>N}, and <sup>15</sup>N solid-state NMR without isotopic enrichment. Quantitative <sup>13</sup>C NMR spectra of the microcapsules and three precursor materials enable determination of the fractions of different components. Spectral editing of non-protonated carbons by recoupled dipolar dephasing, of CH by dipolar DEPT, and of C-N by <sup>13</sup>C{<sup>14</sup>N} SPIDER resolves peak overlap and helps with peak assignment. It reveals that the N- and O-rich resin "imitates" the spectrum of polysaccharides such as chitin, cellulose, or Ambergum to an astonishing degree. <sup>15</sup>N NMR can distinguish melamine from urea and guanazole, NC=O from COO, and primary from secondary amines. Such a comprehensive and quantitative analysis enables prediction of the elemental composition of the resin, to be compared with combustion analysis for validation. It also provides a reliable reference for iterative simulations of <sup>13</sup>C NMR spectra from structural models. The conversion from quantitative NMR peak areas of structural components to the weight fractions of interest in industrial practice is derived and demonstrated. Upon microcapsule formation, <sup>15</sup>N and <sup>13</sup>C NMR consistently show loss of urea and aldehyde and an increase in primary amines while melamine is retained. NMR also made unexpected findings, such as imbedded crystallites in one of the resins, as well as persistent radicals in the microcapsules. The crystallites produce distinct sharp lines and are distinguished from liquid-like components by their strong dipolar couplings, resulting in fast dipolar dephasing. Fast <sup>1</sup>H spin–lattice relaxation on the 35-ms time scale and characteristically non-exponential <sup>13</sup>C spin-lattice relaxation indicate persistent radicals, confirmed by EPR. Through <sup>1</sup>H spin diffusion, the mixing of components on the 2-nm scale was documented.

**Keywords**: Quantitative <sup>13</sup>C NMR, spectral editing, <sup>13</sup>C{<sup>14</sup>N} NMR, amine–aldehyde resin, cross-linked microcapsules, NMR relaxation by persistent radicals

#### Introduction

Solution NMR has long been appreciated by organic chemists for providing the most convincing structural characterization of organic molecules, and it is therefore used routinely to document successful synthesis outcomes.<sup>1,2</sup> However, it is not applicable to insoluble crosslinked polymeric materials. Here, solid-state NMR can play an important role, despite its inherently greater line widths.<sup>3</sup> Like solution NMR, solid-state NMR provides functional-group identification based on chemical shifts governed by systematic trends,<sup>1</sup> spectral editing <sup>4</sup> for peak assignment and resolving spectral overlap, and information on proximity of different components based on couplings between the nuclear spins.<sup>5</sup> NMR resolves more peaks than X-ray photoelectron spectroscopy (XPS) <sup>6</sup> and is intrinsically quantitative,<sup>5,7</sup> unlike many other spectroscopies including infrared and Raman. The high concentration of analyte in the solid state enables relatively fast acquisition of useful <sup>13</sup>C NMR spectra even though the spectral lines are broader than in solution.

Cross-linked industrial polymers are often complex multi-component and multiphasic systems. Solid-state NMR is the best available method for determining their segmental and domain structure. Sufficiently fast quantitative <sup>13</sup>C NMR<sup>7,8</sup> best fulfills the current push by regulatory and patent-granting agencies for a quantitative analytical characterization of commercial materials instead of just a listing of reactants and synthesis conditions. It can also guide synthesis of materials with improved properties by replacing assumptions based on "paper chemistry" with rigorous and quantitative experimental data.

In this paper, a full complement of modern multinuclear solid-state NMR methods 4 is applied to nitrogen-rich resins and related prototypes of formaldehyde-free polymer microcapsules for storage and controlled release of fragrances in cosmetic products. The synthesis of the resin studied here from melamine, urea, and a couple of aldehydes, as well as their further reaction with polymeric colloidal stabilizers, has already been described in the literature. The composition chosen for detailed NMR investigation exhibited particularly good encapsulation properties. The NMR analysis focuses first on the amine–aldehyde resin and its fairly unusual N-containing functional groups. The resin is simple enough for detailed composition analysis using quantitative <sup>13</sup>C NMR<sup>7,8</sup> as well as C-H <sup>10</sup> and C-N <sup>11</sup> spectral editing followed by structural modeling.<sup>12</sup> MultiCP <sup>13</sup>C NMR after recoupled dipolar dephasing <sup>13</sup> separates OCH<sub>3</sub> peaks from overlapping signals. Sharp peaks from liquid-like or from crystalline components can be distinguished based on their dipolar couplings and relaxation properties. The transformation of the resin as it is incorporated into the microcapsules is elucidated by <sup>15</sup>N and <sup>13</sup>C NMR, in particular <sup>13</sup>C { <sup>14</sup>N } SPIDER NMR, <sup>11</sup> which enables separation of strongly overlapping signals of oxygen-bonded amines and polysaccharide rings. The changing melamine: urea ratio and the transformation of secondary to primary amines can

be deduced from  $^{13}$ C,  $^{15}$ N, and  $^{13}$ C{ $^{14}$ N} NMR peak intensities. Based on the quantitative composite-pulse multiCP  $^{13}$ C spectra, $^{8}$  the concentrations of the various components of the microcapsules are determined, as both carbon and weight fractions; their mixing on the nanometer scale is established by  $^{1}$ H spin diffusion in  $^{1}$ H- $^{13}$ C HetCor experiments and  $^{1}$ H inversion recovery. Fast  $T_{1H}$  and fast non-exponential  $T_{1C}$  relaxation indicates the presence of persistent radicals, confirmed by EPR.

# **Experimental**

**Materials**. The resin for microcapsule B9 (Resin-9) was prepared from 9.3 g (74 mmol) of 1,3,5-triazine-2,4,6-triamine (melamine), 13.3 g (222 mmol) of urea, 12.8 g (74 mmol) of 2,2-dimethoxyacetaldehyde (2,2-dimethoxy ethanal or DME), and 42.9 g (296 mmol) of oxalaldehyde (glyoxal), as described in ref.<sup>9</sup>. Two distinct batches of Resin-9 were investigated; they are labeled as Resin-9-1 and -2.

Microcapsules-B9 ( $\mu$ Caps-B) were produced in a Schmizo reactor. An aqueous solution of Ambergum 1221 (carboxymethyl cellulose with one CH<sub>2</sub>COOH group per glucose ring on average according to quantitative <sup>13</sup>C NMR, MW = 90 kg/mol) and a solution of Resin-9 were added to water. The reaction mixture was stirred for 30 min at room temperature (RT) at an adjusted pH. A solution of volatile compounds was added to the reaction mixture and emulsified with an Ultra Turrax at 24 000 rpm at RT for 2 min. An aqueous solution of Alcapsol 144 (a poly(acrylic acid–acrylamide) copolymer, PAA) was added to the emulsion, which was then stirred with an anchor-shaped paddle at 40°C for 1 h, and then at 60°C for 1 h to give a white dispersion. Two distinct batches of  $\mu$ Caps-B were investigated; they are labeled as  $\mu$ Caps-B-1 and -2. Resin-9-2 was used to produce  $\mu$ Caps-B-2. For additional cross-linking, <sup>9</sup> a solution of guanazole was added to the dispersion of  $\mu$ Caps-B-1, which was stirred at 60°C for 1 h, and finally at 75°C for 3 h. The resulting microcapsule dispersion ( $\mu$ Caps-B-GZ) was neutralized with a solution of sodium hydroxide and stored at room temperature.

Elemental analysis. Analyses were performed on a Eurovector EA3000SF Elemental Analyzer (Eurovector, Italy), operating with helium and oxygen at purities of 99.995 % and 99.998 %, respectively. High quality standards were used to establish calibration curves: Sulfanilamide (OAS) for CHNS determination and acetanilide (99 %) for oxygen determination. The sample material was introduced into tin capsules, weighed and packed carefully. The weight of samples was chosen so as to make the absolute content of the detected elements cover all their expected concentration ranges. Calibration samples and analyte samples were dropped into the reactor under constant helium flow for combustion at high temperature. Oxygen was added to ensure complete combustion. Resulting analyte gases (N<sub>2</sub>, CO<sub>2</sub>, H<sub>2</sub>O and SO<sub>2</sub>) were separated by gas

chromatography and analyzed by a thermal conductivity detector. Peak integration was carried out by the Callidus<sup>TM</sup> SW v5.1 software, which provided an element percent report through a linear regression calibration for each sample. Determination of the oxygen content was performed on the same instrument with silver capsules and a specific reactor to operate in pyrolysis mode.

Polarized-light microscopy of Resin-9-2 crystals. A Unitron MPS 12837 microscope with 40x objective (31407) and 10x eyepiece was used for polarized microscopy. A Cole Parmer low-noise illuminator at moderate intensity was used as the light source. The field of view is 0.22 mm in diameter. A thin layer of Resin-9-1 sample was loaded onto a VWR precleaned 25x75 mm micro slide and covered by a Fisherbrand Microscope Cover Glass (24x50-1.5). For ease of transportation, the two ends of the cover glass were taped onto the micro slide. The polarizer was set parallel and perpendicular to the analyzer to obtain light and dark background images, respectively. The images were collected using an iPhone 6s with the lens right above the eyepiece.

**Quantum-chemical prediction of chemical shifts**. Calculation of <sup>13</sup>C NMR chemical shifts was carried out using the Spartan'16 Parallel Suite of Wavefunction Inc., Irvine, CA, USA <sup>14,15</sup>. A conformational search was carried out to obtain a Boltzmann-weighted conformer ensemble employing the Merck Molecular Force Field (MMFF). The resulting ensemble of molecules was further energetically refined at the EDF2/6-31G\* level to finally calculate Boltzmann-weighted <sup>13</sup>C NMR chemical shifts of all conformers in a ~12 kJ/mol energy window.

Single- and double-resonance solid-state NMR. Experiments were performed on a Bruker Avance Neo 400WB NMR spectrometer with  $^{1}$ H and  $^{13}$ C resonance frequencies of 400 MHz and 100 MHz, respectively. Most of the measurements were conducted using a Bruker double resonance magic-angle-spinning (MAS) probe with 4-mm zirconia rotors, except for triple-resonance SPIDER  $^{13}$ C { $^{14}$ N} described in a separate section below. Samples were directly loaded into the rotors, except for the slightly viscous Resin-9 samples, which were loaded into a Kel-F HR-MAS rotor insert. 90° pulse lengths for  $^{1}$ H,  $^{13}$ C, and  $^{15}$ N were 3.6 μs, 4.0 μs, and 6.2 μs, respectively. Two-pulse phase modulation (TPPM)  $^{16}$  with strong  $^{1}$ H decoupling at a field strength of  $\gamma B_1/2\pi = 95$  kHz was used for dipolar decoupling during the Hahn echo  $^{17}$  or total suppression of sidebands (TOSS)  $^{18}$  for dead-time-free detection, while SPINAL-64  $^{19}$  decoupling at  $\gamma B_1/2\pi = 85$  kHz was used during signal acquisition.  $^{13}$ C chemical shifts were referenced to TMS via the carboxyl resonance of α-1- $^{13}$ C-glycine at 176.49 ppm as a secondary reference. All NMR experiments were conducted at approximately 298 K.

A 12.4-ms acquisition time and ~10-s recycle delay were used for Resin-9, and 6.2 ms and 1 s for  $\mu$ Caps-B samples. The typical contact time for ramped (90-100%) cross-polarization (CP) was 1.1 ms. The  $^{13}$ C  $B_1$  field strength used in cross polarization was optimized for each MAS frequency. Quantitative composite-pulse multiCP  $^{8}$   $^{13}$ C NMR spectra were mostly acquired at 14 kHz MAS, except for Resin-9, whose relatively low viscosity made fast spinning not safe enough and was therefore studied at spinning frequencies no higher than 7 kHz. For Resin-9-1, five CP blocks separated by 4  $^{1}$ H repolarization periods (6 s each) were used at 5787 Hz and 512 scans were accumulated for the spectra shown. The signals of the sp<sup>2</sup>-carbons obtained at 5787 kHz MAS need to be scaled up by 1/(1-0.16) = 1.19 to mimic the quantitative spectrum that would have been obtained at 14 kHz, according to spectra of  $\mu$ Caps-B-1 measured at spinning frequencies of 5787 Hz and 14 kHz. A direct polarization spectrum of fast-relaxing  $\mu$ Caps-B-1 was acquired with a recycle delay of 50 s and 1024 scans.  $^{15}$ N NMR spectra were measured with minimal multiCP (two CP blocks of 1.1 ms duration) at 7 – 8 kHz MAS with signal averaging overnight.

CH-only spectra were collected using the dipolar-DEPT pulse program  $^{10}$  at a MAS frequency of 5787 Hz.  $^{13}$ C spectra after  $^{1}$ H inversion recovery and cross polarization  $^{20}$  were measured at 7 and 14 kHz MAS (except for Resin-9 at 5 kHz) to determine the  $^{1}$ H spin–lattice relaxation times  $T_{1\text{H}}$  of various components. The relaxation times at 7 and 14 kHz MAS agreed within  $\pm 15\%$ .

A two-dimensional (2D) <sup>1</sup>H–<sup>13</sup>C heteronuclear correlation (HetCor) spectrum<sup>21</sup> was measured at 7.5 kHz MAS with frequency-switched Lee–Goldburg homonuclear <sup>1</sup>H decoupling,<sup>22</sup> 0.5 ms of Hartmann-Hahn cross polarization with a 90-100% amplitude ramp on the <sup>1</sup>H channel, and TOSS before detection. The experiment was also performed with a mixing time of 10 ms before CP, to allow for <sup>1</sup>H spin diffusion over a few nanometers.

**Triple-resonance SPIDER** <sup>13</sup>C{<sup>14</sup>N} **NMR.** SPIDER <sup>13</sup>C{<sup>14</sup>N} NMR experiments <sup>11</sup> were performed using a 19-year-old Bruker triple-resonance probe, in a 4-mm rotor at 5 kHz spinning frequency, with ca. 70 kHz <sup>1</sup>H decoupling, a <sup>14</sup>N radio-frequency field strength of roughly  $\gamma_N B_1 = 2\pi \times 30$  kHz, and 6-μs <sup>13</sup>C 180° pulse length. In the center of a 1.6-ms period with pulsed recoupling of <sup>14</sup>N–<sup>13</sup>C dipolar interactions using <sup>13</sup>C 180°-pulses every half rotation period, pulsed saturation of <sup>14</sup>N was applied for 0.8 ms at 160 W with a train of 4 μs pulses and 2 μs windows.<sup>11</sup>

**Simulation of <sup>13</sup>C spectra from structural models.** The ACD/C+H/X NMR predictor was employed to simulate the <sup>13</sup>C and <sup>15</sup>N spectra of the compounds in structural models, in addition to the quantum-chemical calculations described above. Gaussian line broadening of ca. 5 ppm

for <sup>13</sup>C and 10 ppm for <sup>15</sup>N was added using a MATLAB Script. In the simulated spectra after dipolar dephasing, the peak intensities of CH and CH<sub>2</sub> groups were set to zero, while those of methyl and quaternary carbons were reduced to 50% and 90%, respectively. Each combination the proposed structural components of Resin-9-1 with a specific mixing ratio produced two simulated <sup>13</sup>C spectra (with and without dipolar dephasing). The best mixing ratio was found by minimizing the mean-square-deviation between the simulated and the experimental spectra.

#### Results

**Resin-9-1.** Figure 1 shows the nearly quantitative <sup>13</sup>C NMR spectrum of Resin-9-1 without and with dipolar dephasing, as well as a CH-only<sup>10</sup> spectrum, while Figure 2 displays a selective spectrum of C bonded to N obtained by SPIDER <sup>13</sup>C{<sup>14</sup>N} NMR. Most of the strongest signals are seen to be due to CH bonded to N, which is not surprising given the nitrogen-rich reactants. Clear exceptions are the signals at 106 and 57 ppm, which are assigned to O-CH-O and OCH<sub>3</sub>, sites that indeed cannot accommodate bonding to N since O and H saturate all four valences of C. On the basis of the known reactants (see Figure 1a), chemical-shift trends, and spectral editing, the signals at 167, 162, 106, 84, 76 and 57 ppm can be assigned to melamine rings, urea N-(C=O)-N, O-CH-O, N-CH-O-C, N-CH-O-, and O-CH<sub>3</sub>, respectively. Similar chemical shifts have been reported in the literature for hardened melamine–glyoxal resins.<sup>23</sup>

MultiCP <sup>15</sup>N NMR of Resin-9-1, see Figure 3, provides a complementary view of its nitrogen bonding environment. The left-most peak, at 170 ppm, is from the ring nitrogen in melamine. The shoulder at 120 ppm can be assigned to tertiary amine, in part based on its slower dipolar dephasing when <sup>1</sup>H decoupling has been gated off for 280 μs. The absence of an amide <sup>13</sup>C NMR signal at 173 ppm, see Figures 1b 2b, precludes assignment of the 120-ppm <sup>15</sup>N signal in Figure 2 to amides. The resonances at 103 and 82 ppm can be assigned to secondary and primary amines, respectively, that are bonded to sp<sup>2</sup>-hybridized C, which gives a downfield shift of ~ +40 ppm compared to sp<sup>3</sup>-C-bonded amines. Specifically, the 82-ppm signal agrees closely with the 84 ppm chemical shift of the primary amine groups of melamine.<sup>6</sup>

Crystalline component in Resin-9-2. Figure 4 shows multinuclear NMR spectra of Resin-9-2. In the  $^{13}$ C and  $^{15}$ N spectra, a small number of intense sharp peaks are prominent, in addition to broad signals as in Resin-9-1. Sharp peaks can be due to liquid-like or crystalline components. Due to the different molecular mobilities in these environments, their dipolar couplings and relaxation times are drastically different and enable unambiguous assignment to liquid or crystal. Liquid-like components have weak static C-H dipolar couplings and fast  $T_{1H}$  and  $T_{1C}$  relaxation, due to dipolar fields fluctuating fast and with large amplitudes. The signal at 84 ppm disappears completely within 40  $\mu$ s of dipolar dephasing, see Figure 4a, lower trace, proving

solid-like  ${}^{1}\text{H}$ - ${}^{13}\text{C}$  dipolar couplings. A very long  $T_{1\text{H}}$  relaxation time of ~30 s, compared to ~2 s of the broad components, confirms the assignment to a rigid solid, as does the wide  ${}^{1}\text{H}$  spectrum of the slowly-relaxing components, see Figure 4d. The crystallites must be of significant size (>50 nm), since in nanosized crystallites,  ${}^{1}\text{H}$  spin diffusion would equalize the  $T_{1\text{H}}$  of all rigid components on the 5-s time scale. The inset in Figure 4c shows a polarized-light micrograph where sub-millimeter-sized crystals are clearly observed, confirming the conclusions from NMR. The sharp peaks of the crystalline component account for 37  $\pm$  5 % of the spectral area in Figure 4b.

**Spectroscopic characterization of μCaps-B**. Figure 5 shows <sup>13</sup>C NMR spectra of μCaps-B-1 and -2, produced by reacting different batches of Resin-9 with Ambergum, a polysaccharide with O-CH<sub>2</sub>-COO side groups, under vigorous stirring and subsequently with Alcapsol, a polyacrylic acid-acrylamide copolymer (PAA). The spectra of the two neat polymeric components are superimposed for reference in Figure 5 (dashed lines); the PAA backbone CH/CH<sub>2</sub> signals are seen to be quite well resolved from other peaks and can therefore be used for quantifying the Alcapsol content.

Peak assignment was further assisted by spectral editing (see Figure S1). Dipolar dephasing for identifying non-protonated C and CH<sub>3</sub> groups shows that resonances at >140 ppm are from non-protonated C, while the small OCH<sub>3</sub> peak at 55 ppm resolved after dipolar dephasing enables an estimate of the extent of incorporation of DME (see structure in Figure 1a). Dipolar DEPT for CH selection in Figure S1b shows that the signal between 45 and 110 ppm is mostly from CH moieties, except for some OCH<sub>2</sub> groups resonating between 60 and 80 ppm. While the observed signals at >70 ppm can be attributed to ethers (C-O-CH<sub>2</sub>), the 62-ppm polysaccharide (Ambergum) CH<sub>2</sub>-OH signal is rather weak. Most importantly, spectral editing by SPIDER <sup>13</sup>C {<sup>14</sup>N} NMR resolves the overlap between the N-CH-O peaks of the resin and the C-CH-O signals of the polysaccharide (Ambergum), see Figures 6 and S2. The positions of the N-CH-O peaks at 84 and 76 ppm match those in Resin-9, but the relative peak intensities are modified, with a reduced intensity around 84 ppm. Similarly, pronounced changes from Resin-9 are observed in the <sup>15</sup>N NMR spectra of μCaps-B in Figures 3 and S3.

**Component mixing in μCaps-B from <sup>1</sup>H spin diffusion**. μCaps-B consists of at least three oligomeric or polymeric components: Resin-9, Ambergum, and Alcapsol (PAA). <sup>1</sup>H spin diffusion can be used to assess mixing or domain sizes of these components, from the 0.5-nm to the 30-nm scale. Here we show how mixing can be proved by <sup>1</sup>H-<sup>13</sup>C HetCor NMR even in complex multicomponent materials with extensive peak overlap.

The HetCor spectrum of  $\mu$ Caps-B-2 in Figure 7a was obtained with a moderate cross-polarization time of 0.5 ms and no separate spin diffusion delay. The nonpolar alkyl (mostly PAA backbone)  $^{13}$ C resonances at < 50 ppm correlate with protons at < 3 ppm, as expected. It is interesting to note the  $^{1}$ H chemical shifts of  $\sim$ 6 ppm of the 75 and 84 ppm signals, which are distinct from the  $\sim$ 4.2 ppm  $^{1}$ H chemical shifts of polysaccharides but in agreement with the N-CH-O moieties identified as dominant by  $^{13}$ C  $\{^{14}$ N $\}$  SPIDER NMR.

After 10 ms of <sup>1</sup>H spin diffusion, all these spectral differences have been erased, see Figure 7b. All vertical cross sections show the same spectral line shape, as do all horizontal ones, see Figure 7b, right hand side. This is the hallmark of magnetization equilibration in a finely mixed system, with domain sizes < 5 nm. For instance, the cross section at 2 ppm in the <sup>1</sup>H dimension shows that <sup>1</sup>H magnetization from PAA has reached the amine-rich resin and Ambergum to the same extent as PAA itself.

<sup>1</sup>H inversion recovery (<sup>13</sup>C-detected) of μCaps-B. <sup>1</sup>H spin diffusion is also operative during <sup>1</sup>H spin–lattice relaxation. <sup>1</sup>H inversion recovery with cross polarization and <sup>13</sup>C detection shows the same fast relaxation for all components in μCaps-B-1, see Figure 8. This includes more than 30 times faster relaxation of Ambergum and PAA in μCaps-B-1 compared to neat Ambergum and PAA, see Figure 9. It is particularly noteworthy that all components cross zero at the same time, see Figure 8 (vertical center). This must be attributed to fast erasure of any differential <sup>1</sup>H relaxation by <sup>1</sup>H spin diffusion in a very finely mixed system, probably combined with proximity to the same drivers of spin–lattice relaxation.

Fast spin–lattice relaxation and persistent radicals in  $\mu$ Caps-B. The  $T_{1H}$  relaxation time of 0.036 s in  $\mu$ Caps-B-1 is remarkably short, 50 and 100 times shorter than in neat Ambergum and Resin-9, respectively. The fast relaxation cannot be attributed to the fluctuating fields produced by bound water, since the amount of bound water, recognized as a fairly sharp peak of short  $T_{1\rho}$  in  $^{1}$ H NMR (Figure S4), does not correlate with  $T_{1H}$ . Indeed, the fluctuating fields of a moderate amount of bound  $H_{2}$ O are not strong enough to drive  $T_{1H}$  relaxation on the 30-ms scale.

The most likely drivers of the observed fast  $^{1}$ H spin—lattice relaxation are persistent radicals distributed throughout the microcapsule material. $^{24,25}$  The large magnetic moment of unpaired electrons produces large dipolar fields at the nuclei, which fluctuate with rates near the nuclear Larmor frequency due to electron spin—lattice relaxation. The hypothesis is confirmed by additional observations. Fast non-exponential  $T_{1C}$  relaxation of all components is observed in  $\mu$ Caps-B-1, see Figure S5, which is characteristic of unpaired electrons (free radicals),  $^{24,25}$  arising from the superposition of faster relaxation of  $^{13}$ C near an unpaired electron with slower

relaxation of  $^{13}$ C at a larger distance from any radical. The slightly faster relaxation of OCH/NCH signals compared to the C=N peaks suggests that the unpaired electrons tend to be closer to the former than the latter. The conclusive method for detecting persistent radicals is EPR spectroscopy. Figure S6 shows the EPR spectrum of  $\mu$ Caps-B-1 with significant intensity from organic radicals.

In  $\mu$ Caps-B-2,  $T_{1H}$  relaxation is less fast ( $T_{1H}$  = 0.22 s), but it is still 10 times faster than in the corresponding Resin-9-2 ( $T_{1H}$  = 2.1 s in the broad amorphous and ~30 s in the sharp crystalline component), see Figure S7.

# **Discussion**

Confirmation of quantitative <sup>13</sup>C NMR. The quantitative composition analysis rests on multiCP <sup>13</sup>C NMR providing quantitative peak intensities. From measurements of peak-integral ratios in spectra of model compounds, the multiCP method is known to provide nearly quantitative peak areas, with  $\pm 5\%$  uncertainty <sup>7,8</sup> (meaning, for instance, that the signal of one of ten resolved sites would show a peak intensity of  $(10 \pm 0.5)\%$ . This quantitative quality of multiCP could be tested and confirmed for the systems studied here using  $\mu$ Caps-B-1 with its unusually fast  $T_{1C}$  relaxation, which makes it possible to record a nearly quantitative direct-polarization (DP) spectrum with a 50-s recycle delay and an adequate signal-to-noise ratio. Figure S8 compares the multiCP and DP <sup>13</sup>C NMR spectra of  $\mu$ Caps-B-1. The spectral line shapes agree well, showing that the multiCP <sup>13</sup>C NMR spectrum is quantitative. Closer inspection indicates that the difficult-to-cross-polarize melamine peak is actually relatively stronger after multiCP than DP; this can be attributed to incomplete relaxation of this signal within the 50-s recycle delay of the DP experiment. This suggests that in this instance, the multiCP spectrum not only provides a better signal-to-noise ratio (better precision) but also slightly higher accuracy than the 50-s DP spectrum.

**Table 1**. Functional group composition of Resin-9-1 from NMR and in the combined structural models (oligomers 9a-c) of ref.<sup>9</sup>

Funct.	COO	Mel-	Ur	·ea	Im-	$OC_{np}O$	ОСНО	NCHOC	NCHO	OCH <sub>3</sub>	NCH	?
group	NCO	amine			ine						?	
Chem.	180	167	>160	<160	162	100-110	) ppm	84 ppm	74	57	62	50
shift	ppm	ppm	ppm	ppm	ppm				ppm	ppm	ppm	ppm
%C	3%	17%	10%	6%	1%	3%	6%	24%	16%	9%	4%	2%
%C in	3%	58%	14	<b>%</b>	3%	0%	0%	0%	8%	0%	11%	3%
ref. <sup>9</sup>												

**Functional-group composition of Resin-9 from NMR**. The bonding partners of carbon in the sites producing the major resonances of Resin-9 have been identified through spectral editing and major chemical-shift trends. For instance, the carbon resonating at 84 ppm is bonded to one hydrogen atom, according to dipolar DEPT, to nitrogen according to SPIDER NMR, and to one oxygen according to the chemical shift. The fourth bonding partner must be carbon. The composition in terms of functional groups determined in this way is summarized in Table 1.

Elemental composition of Resin-9 from NMR. Spectral editing has identified all bonding partners (H, O, N, C) of carbon producing the main resonances in Figure 1b. On that basis, the elemental composition of Resin-9-1 can be estimated. In this analysis, bonding of certain heteroatoms to two carbons needs to be properly considered: Since the amines are either bonded to the melamine ring or to the urea C=O moiety, their nitrogen can be counted fully with respect to the "core" sp²-hybridized carbon signals and should not be considered again when the N-CH-O signals are analyzed. Oxygen in OH groups occurs in a 1:1 ratio with the attached C-OH carbon, while ether oxygen is shared between two C and therefore counted only half with each C-O-C carbon. Table S1 summarizes this analysis.

This approach enables us to use the only other quantitative composition information available for these complex insoluble organic materials, elemental analysis by combustion, to validate the NMR results or reveal potential blind spots or mis-assignments. In other words, we can test the quality of the NMR analysis by comparing the NMR-predicted elemental composition with combustion CHN data. As shown in Table S1, 102 carbon atoms are associated with 66 N, 65 O, and about 175 H atoms, with a total mass of 3363 Da. Converted to wt%, this yields 36% C, 27% N, 31% O, and  $\sim$ 5.2 % H. The C:N mass ratio of 1.33  $\pm$  0.03 from NMR is in good agreement with that from combustion analysis (1.32  $\pm$  0.02), see Table S2.

**Structural model of Resin-9**. Figure 10 displays two structural models of Resin-9 and the corresponding simulated <sup>13</sup>C NMR spectra. The first model, see Figure 10a, is from the literature <sup>9</sup> and does not match the experimentally observed sp<sup>3</sup>-carbon peaks in the experimental NMR spectrum. Spectral editing by dipolar dephasing, see Figure 10b, also shows that the one sp<sup>3</sup>-carbon peak that is matched by the model is from a different type of functional group (OCH<sub>3</sub> in the experiment instead of N-CH-N aminal in the model).

The second model, see Figure 10c, was optimized to match the <sup>13</sup>C NMR spectra, see Figures 10d,e, and also accounts for the peaks in the <sup>15</sup>N spectrum, see Figure S10. It postulates four main components, including two diastereomers of a tricyclic molecule, see Figure 11, that can account for the observed sharp peaks at 162 and 84 ppm in the <sup>13</sup>C spectrum and at 104 ppm in the <sup>15</sup>N spectrum of Resin-9-2, and is easily derived from urea and glyoxal. Quantum-

chemical calculations of the nonplanar tricyclic molecule have indicated that the chemical shifts of the four N-CH-O stereocenters vary from 78 to 85 ppm depending on the relative configuration of five possible diastereomers (Figure 11), which can account for the peaks at 76 and 84 ppm in the experimental spectrum. The molar masses of the three components in the model of Figure 10c are within the range observed experimentally in ref.<sup>9</sup>. While most of the primary amines are from melamine, at least 1/3 of the amine of melamine must be secondary to ensure covalent incorporation of melamine into the resin, as shown in the model.

Imine ruled out by gated decoupling. Imine (N=CH-R) formation in Resin-9 from glyoxal has been proposed in the literature. Imine is unusual as a CH moiety resonating at a high chemical shift of 162 ppm. It would be suppressed by dipolar dephasing, but no such signal suppression near 162 ppm is significantly observed in Figure 1b, which is NMR evidence against significant imine concentration in Resin-9. This finding is not unexpected since reaction with  $H_2O$  (N=CHR +  $H_2O$   $\rightarrow$  HN-CHR-OH) can convert imines to the types of functional groups prominently observed in Resin-9.

**Resin-9 vs. polysaccharides**. The spectrum of Resin-9-1 in Figure 1b between 120 and 50 ppm looks deceptively similar to the typical pattern of a polysaccharide. For instance, Resin-9-1 as well as cellulose and chitin show resonances near 105, 87, 75, and 62 ppm. As a result, in  $\mu$ Caps-B materials the resonances of O-CH-O and CH-O segments derived from Resin-9 and of the polysaccharide Ambergum overlap nearly completely. Spectral editing, in particular  $^{13}$ C $\{^{14}$ N $\}$  NMR, see Figure 2, is indispensable for resolving this overlap.

Urea: melamine amine ratio. The ratio of the two amine compounds can be estimated from both  $^{13}$ C and  $^{15}$ N NMR. The sp<sup>2</sup>-carbon signal ratio  $c_{\text{Mel}}$ :  $c_{\text{Ur}}$  can be determined directly from the  $^{13}$ C spectrum where peaks at 167 and <164 ppm, respectively, are often quite well resolved. However, the ratio of the concentrations of the reactive amine groups of the two compounds, amn<sub>Ur</sub>: amn<sub>Mel</sub>, is more interesting structurally than the carbon ratio. The two ratios differ by a factor of two.

$$\operatorname{amn}_{\operatorname{Ur}} : \operatorname{amn}_{\operatorname{Mel}} = 2 \ c_{\operatorname{Ur}} : c_{\operatorname{Mel}} \tag{1}$$

with one amine per carbon in melamine, but two amines per carbon in urea. In Resin-9-1, the  $sp^2$ -carbon ratio gives  $amn_{Ur}$ :  $amn_{Mel} = 1.9$ : 1, so urea provides most amine groups, while in  $\mu$ Caps-B-1 and -2 the ratio is lower, 1.44: 1 and 0.77: 1, respectively, with a larger amine contribution from melamine.

The melamine: urea ratio is also reflected in the  $^{15}$ N spectrum, where the '=N' signal intensity  $n_{\text{Mel}}$  of melamine at 170 ppm is a well-resolved, suitable reference. Since the other melamine N (with amn<sub>Mel</sub> =  $n_{\text{Mel}}$ ) and both N of urea contribute to the bands at <150 ppm (signal fraction 'am', for amines plus amides), we can equate

$$am - amd = amn_{Mel} + 2 amn_{Ur} = n_{Mel} + 2 amn_{Ur}$$
 (2)

where the relatively small intensity of amide of PAA (which can be estimated based on  $^{13}$ C NMR) was included as 'amd'. Dividing both sides by  $n_{\text{Mel}} = \text{amn}_{\text{Mel}}$ , we can obtain the ratio of the two types of amines in terms of  $^{15}$ N spectral intensities,

$$amn_{Ur}$$
:  $amn_{Mel} = \frac{1}{2} (am - amd)/n_{Mel} - \frac{1}{2}$  (3)

Applying eq.(3) to Resin-9-1, with am/ $n_{Mel}$  = 84/16 (±4) from the <sup>15</sup>N spectrum and amd = 0 since there is no amide, yields amn<sub>Ur</sub>: amn<sub>Mel</sub> = (2.1 ± 0.3) : 1, in agreement with the result from <sup>13</sup>C NMR. In  $\mu$ Caps-B-2, am/ $n_{Mel}$  = 73/27 = 2.7 from the <sup>15</sup>N spectrum while <sup>13</sup>C NMR shows that amd/ $n_{Mel}$   $\approx$  (3±1.5)/26 = 0.12 ± 0.06 (assuming acrylate:acrylamide = 50:50 ± 25 in Alcapsol). This yields amn<sub>Ur</sub>: amn<sub>Mel</sub> = 0.79 : 1 (± 0.03), in good agreement with the result from <sup>13</sup>C NMR, confirming loss and reduced importance of urea in the microcapsule.

**Primary amine fraction**. The NH<sub>2</sub> (primary amine) fraction can be estimated directly from the area fraction of the right-most peak in the <sup>15</sup>N spectra of Figures 3 and S3, near 85 ppm, but is also reflected in the relative intensity of the sp<sup>3</sup>-C-N signal, taking the distinctive melamine peak at 167 ppm as a reference. With two nitrogen-bonded sp<sup>3</sup>-hybridized carbons per N<sub>t</sub> (tertiary amine, <sup>15</sup>N signal fraction  $n_t$ ) and one N-bonded sp<sup>3</sup>-carbon per NH (2° amine, signal fraction  $n_H$ ), we can equate <sup>15</sup>N and <sup>13</sup>C peak intensity ratios:

$$(2 n_{\rm t} + n_{\rm H})/n_{\rm Mel} = {\rm sp}^3 c_{\rm N}/c_{\rm Mel}$$
 (4)

where  $sp^3c_N$  is the  $^{13}C$  signal fraction of  $sp^3$ -hybridized C bonded to N.

The larger the primary-amine fraction  $n_{\rm H2}$  (which does not contribute any N-bonded sp<sup>3</sup>-hybridized carbon) the smaller the other fractions  $n_{\rm t}$  and  $n_{\rm H}$  and therefore the sp<sup>3</sup> $c_{\rm N}/c_{\rm Mel}$  ratio in  $^{13}{\rm C}$  NMR. The total amine plus amide  $^{15}{\rm N}$  fraction (am) can be expressed in terms of the tertiary, secondary, and primary amine concentrations  $n_{\rm t}$ ,  $n_{\rm H}$ , and  $n_{\rm H2}$ , respectively:

$$am = n_t + n_H + n_{H2} + amd$$
 (5)

Inserted into eq.(4) this gives

$$(n_{\rm t} + {\rm am - amd - } n_{\rm H2})/n_{\rm Mel} = {\rm sp}^3 c_{\rm N}/c_{\rm Mel}$$
 (6)

which shows the opposing trends of primary-amine concentration  $n_{\rm H2}$  and N-bonded sp<sup>3</sup>-carbon concentration sp<sup>3</sup> $c_{\rm N}$  explicitly.

In Resin-9-1, according to Figure 3 we have a primary amine fraction of  $n_{\rm H2} = 20\%$ , while  $n_{\rm t} = (18 \pm 4)\%$ ,  $n_{\rm H} = 44\%$ , and  $n_{\rm Mel} = (16 \pm 4)\%$ , which predicts sp $^3c_{\rm N}/c_{\rm Mel} = (5 \pm 2)$  according to eq.(4), while the  $^{13}$ C NMR spectrum and Table 1 shows sp $^3c_{\rm N}/c_{\rm Mel} = 2.7$ . In  $\mu$ Caps-B-2, the primary amine fraction is  $n_{\rm H2} = (31 \pm 4)\%$ , while  $n_{\rm t} = 7\%$ ,  $n_{\rm H} = (33 \pm 4)\%$  (corrected for the small amide fraction), and  $n_{\rm Mel} = 27\%$ , so eq.(4) predicts sp $^3c_{\rm N}/c_{\rm Mel} = 1.7 \pm 0.4$ , while the SPIDER spectrum after scaling suggests sp $^3c_{\rm N}/c_{\rm Mel} \approx 1.3$ . Thus  $^{15}$ N and  $^{13}$ C NMR agree that upon microcapsule formation the primary amine fraction increases and therefore the N-bonded sp $^3$ -carbon fraction decreases. This unexpected result is directly confirmed by comparison of the SPIDER spectra of Resin-9-1 and  $\mu$ Caps-B-2 in Figures 2 and 6, which shows a pronounced reduction in sp $^3$ -C-N signals (at < 100 ppm) relative to the melamine sp $^2$ -C band.

**DME incorporation**. Two different aldehydes, glyoxal and methoxy-containing DME (shown in Figure 1a), were used in the synthesis of Resin-9. The concentration of DME incorporated into the resin and microcapsules can be assessed based on its OCH<sub>3</sub> signal near 55 ppm, which is best resolved after dipolar dephasing, see the bottom traces in Figures 1b and S1a. The DME structure in Figure 1a makes it clear that for each two OCH<sub>3</sub> carbons, DME also contributes an O-CH-O- di-ether moiety resonating near 108 ppm. In the spectrum of Resin-9-1 (Figure 1b), the observed OCH<sub>3</sub>:-O-CH-O-signals indeed match the predicted 2:1 ratio within the experimental uncertainty.

**Transformation of Resin-9 in \muCaps-B**. Through the quantitative and semi-quantitative multinuclear NMR spectra presented here, e.g. in Figures 1, 5, 6, S1, S2, and S9 as well as Tables 1 and 2, the transformation of amines and carbons of Resin-9 upon incorporation in  $\mu$ Caps-B can be monitored. Melamine becomes a major component of  $\mu$ Caps-B, while urea is relatively depleted compared to Resin-9. Quantitatively applying eqs.(1) and (3), the urea : melamine amine ratio changes from 2:1 in Resin-9 to 1.4 : 1 in  $\mu$ Caps-B-1 and 0.8 : 1 in  $\mu$ Caps-B-2. This might be attributed to trifunctional melamine being better retained in the microcapsules than the only difunctional urea. The urea peaks are significantly shifted, from

>162 to <162 ppm, as Resin-9 is incorporated in µCaps-B, see Figures 1b, 5 and S9. Both of these observations indicate transformation of the tricyclic urea ether (see Figure 10c) prominent in Resin-9.

In Resin-9, a large fraction of urea amine is secondary and resonates near 100 ppm in the  $^{15}N$  NMR spectrum, presumably in structures similar to those shown in Figure 11, with the corresponding strong N-CH-O-C  $^{13}C$  resonance near 84 ppm. The increased fraction of primary amine observed in the  $^{15}N$  NMR spectra of  $\mu Caps$ -B compared to Resin-9, see Figures 3 and S3, indicates that a large fraction of melamine and urea amine groups are 'freed' upon incorporation into the microcapsule. Accordingly, the fraction of sp³-hybridized C bonded to N between 70 and 90 ppm is much lower in  $\mu Caps$ -B than in Resin 9 when compared on the basis of the melamine ring carbons, see Figure S9. As shown above using eq.(4), the ratio of sp³-hybridized C-N to melamine C drops from  $\sim 3:1$  in Resin-9 to 1.5:1 in  $\mu Caps$ -B-2, which was not expected.

Component quantification in μCaps-B. Based on quantitative <sup>13</sup>C NMR spectra, the components of a composite material can be quantified by integration or deconvolution. The melamine peak at 167 ppm provides straightforward quantification of this robust reactant. The PAA content of μCaps-B can be determined quite accurately from the well-resolved backbone CH/CH<sub>2</sub> band of PAA near 40 ppm; the side-group (C=O) carbon is taken into account by multiplying with 1.5; the experimental value for neat PAA is 1.49, confirming that that the multiCP spectrum of PAA is quantitative. The PAA peaks are shifted to the right in μCaps-B-1 relative to neat PAA; the reproducibility of this shift was tested explicitly. Other signals also appear to undergo a similar shift to lower ppm values, which might be due to effects of the persistent radicals. No systematic peak shift was observed in μCaps-B-2.

The Ambergum content is more difficult to ascertain since no Ambergum peak is fully resolved from the other components, though the COO peak near 177 ppm is quite clear when the Ambergum fraction is high, see Figure 5a. From the SPIDER  $^{13}C\{^{14}N\}$  spectra we can conclude that the Ambergum-overlapping N-CH-O signals between 70 and 90 ppm are of similar intensity in  $\mu$ Caps-B-1 and -2 and must account for 10-20% of the quantitative  $^{13}C$  spectrum. Upper limits to the Ambergum fraction in  $\mu$ Caps-B-1 and -2, of  $\leq$ 37% and  $\leq$ 25%, respectively, are obtained from the total  $^{13}C$  intensity between 60 and 110 ppm (see Table 2) corrected for a minimum of 10% C-N and taking into account the eighth carbon resonating near 177 ppm. The approximate deconvolution shown in Figure 5, based significantly on the Ambergum COO peak near 177 ppm, indicates that the Ambergum content of the two microcapsules differs by about a factor of 2.5, while the fraction of N-bonded aldehyde-derived

carbons from Resin-9 is similar, consistent with the SPIDER  $^{13}C\{^{14}N\}$  spectra. In  $\mu$ Caps-B-2, Ambergum accounts for approximately 30% of the signal intensity between 60 and 110 ppm (~10 %C), while glyoxal- and DME-derived C accounts for ~70%. In  $\mu$ Caps-B-1, the estimated Ambergum content is  $26 \pm 6$  %C.

The carbon fractions of the components of  $\mu$ Caps-B-1 and -2 determined in this analysis are listed in Tables 2 and 3. On this basis, the weight fractions can be quantified based on the known elemental compositions of the components and the measured elemental composition of the overall material, as described below. As an alternative to the integration-based approach used here, deconvolution has also been applied to the spectrum of  $\mu$ Caps-B-2, as shown in Figure S11 and discussed at the end of the Supporting Information.

**Table 2**. Functional group composition (%C) of μCaps-B-1 and -2.

Funct.	COO	Mel-	Urea	C=C	O-C-	N-	О-СН	ОСН	PAA	Mob.	PAA
group		am-			O	СН-		2	CH/	alkyl	
		ine				О-С		etc.	$CH_2$		
Chem.	190-	170-	164 -	148	110 -	95 -	80 -	65 -	52 -	35-10	52–32
shift	170	164	148	-110	95	80	65	52	32		&
(ppm)											~177
μCaps-	11%	18%	13%	3%	5.5%	9%	22%	6.5%	10%	≤1%	14.9%
B-1											
μCaps-	7.5%	27%	10%	7%	3%	7%	18%	4.5%	13%	3%	19.4%
B-2											

**Table 3**. Component weight fractions (in wt%) of different components in  $\mu$ Caps-B-2 ( $e_{C,tot} = 0.34$ , see Table S3) calculated from <sup>13</sup>C NMR peak intensities (in %C) and carbon fractions  $e_C$  from elemental analysis or molecular formulas, based on eq.(10).

Component	Melamine	Urea	Alcapsol	Glyoxal- &	Ambergum	Mob.	C=C	Tot.
	ring +	O=C	(PAA)	DME-	(incl.	alkyl		
	$(NH_{1.5})_3$	(NH) <sub>2</sub>		derived C-O	COO)			
e <sub>C</sub> C fract.	0.29	0.21	0.51	~0.37	0.43	~0.8	~0.9	
c <sub>X</sub> (%C)	27%	10%	19.4%	~0.7 × 32%	~0.3 ×	3%	7%	100%
					32%×8/7			
w <sub>X</sub> (wt%)	32%	16%	13%	~21%	~9%	1%	3%	95%

Reproducibility of  $\mu$ Caps-B synthesis. Comparison of the spectra of  $\mu$ Caps-B-1 and -2 shows the same component signals (of melamine, urea, Ambergum, Alcapsol, etc.), but in different

proportions. Urea is similarly transformed in both samples relative to Resin-9. Taking melamine and PAA as a reference, there is less urea, Ambergum, and DME in  $\mu$ Caps-B-2. There is also more perfume oil left in  $\mu$ Caps-B-2 (relatively sharp peaks between 10 and 35 ppm). Peak shifts to the right, which were verified by replicate experiments and might be related to the high concentration of persistent radicals, were observed in  $\mu$ Caps-B-1 but not -2.

Conversion from <sup>13</sup>C NMR intensities to weight fractions. The fractional peak area of a certain structural component in a quantitative <sup>13</sup>C NMR spectrum is the *carbon* fraction (%C) of that component. In industrial practice, the actual mass or weight fractions are of interest. We show here that the weight fractions can be obtained easily from the NMR peak areas combined with elemental composition data (specifically the carbon mass fractions). In the following, we choose PAA as a specific component for clarity, but the equations apply analogously to any other component.

The carbon fraction  $f_{C,PAA}$  (peak area in %C) of PAA is the ratio of the carbon masses  $m_{C,PAA}$  of PAA and  $m_{C,tot}$  of the total sample:

$$f_{C,PAA} = m_{C,PAA} / m_{C,tot}$$
 (7)

The carbon masses can be related to the corresponding full masses via the elemental carbon fractions  $e_{\text{C,PAA}}$  and  $e_{\text{C,tot}}$  according to

$$m_{\text{C,PAA}} = e_{\text{C,PAA}} m_{\text{PAA}}$$
 (8a)

$$m_{\text{C,tot}} = e_{\text{C,tot}} m_{\text{tot}}$$
 (8b)

Combining eqs. (8a,b) solved for  $m_{PAA}$  and  $m_{tot}$ , the weight fraction  $w_{PAA} = m_{PAA}/m_{tot}$  can be reexpressed in terms of the NMR-based carbon fraction  $f_{C,PAA}$  and the elemental compositions of PAA and the sample overall:

$$w_{\text{PAA}} = m_{\text{PAA}}/m_{\text{tot}}$$

$$= (m_{\text{C,PAA}}/e_{\text{C,PAA}})/(m_{\text{C,tot}}/e_{\text{C,tot}})$$

$$= f_{\text{C,PAA}} (e_{\text{C,tot}}/e_{\text{C,PAA}})$$
(9)

Since  $f_{C,PAA}$  is equal to the fractional integral <sup>13</sup>C NMR intensity  $c_{PAA} = I_{PAA}/I_{tot}$ , we can write the relation between weight fraction  $w_{PAA}$  and <sup>13</sup>C NMR intensity fraction  $c_{PAA}$  as

$$w_{\text{PAA}} = c_{\text{PAA}} \left( e_{\text{C,tot}} / e_{\text{C,PAA}} \right) \tag{10}$$

The elemental carbon mass fraction  $e_{C,PAA}$  can be calculated from the known chemical structure of PAA, while  $e_{C,tot}$  of the sample overall is best determined by combustion analysis. Eq.(10) shows that if the carbon content of the component matches that of the sample overall, the  $^{13}C$  NMR peak area fraction is equal to the weight fraction, as expected. On the other hand, if the component is relatively rich in heteroatoms, its weight fraction is larger than the  $^{13}C$  intensity fraction since the heteroatoms contribute to the mass but not to the  $^{13}C$  NMR intensity. Accordingly, in this case  $e_{C,PAA} < e_{C,tot}$  gives  $w_{PAA} > c_{PAA}$  in eq.(10). The application of eq.(10) to determine the composition of  $\mu$ Caps-B-2 in wt% is demonstrated in Table 3, using the elemental analysis data of Table S3. The differences between corresponding carbon and weight fractions are seen to be significant.

<sup>1</sup>H-<sup>13</sup>C HetCor NMR of μCaps-B: Component mixing. The signals of melamine, urea, aldehyde-derived C, Ambergum, and PAA in μCaps-B equilibrate within 10 ms of <sup>1</sup>H spin diffusion in the <sup>1</sup>H-<sup>13</sup>C HetCor spectrum of Figure 7b. The conversion from this time scale to the length scale of mixing is achieved based on the <sup>1</sup>H spin diffusion coefficient, which has a value of  $D \approx 0.6$  nm<sup>2</sup>/ms in rigid proton-rich polymers. <sup>26,27</sup> Magnetization will diffuse by less than  $x_{rms} = \sqrt{2Dt_{se}} \le 4$  nm within a spin exchange time  $t_{se}$  of 10 ms. Thus, since equilibration is observed across components within 10 ms of exchange time, they must be finely mixed on a scale of a few nanometers. The extremely homogeneous and fast  $T_{1H}$  relaxation in μCaps-B-1, see Figure 8, confirms this conclusion.

**Persistent radicals in μCaps-B**. The unexpected presence of persistent radicals in μCaps-B-1 was indicated by a drastic acceleration of  $T_{1H}$  relaxation and by fast non-exponential  $T_{1C}$  relaxation. EPR confirmed the existence of unpaired electrons. They can be tentatively assigned as stabilized mechanoradicals generated by the extreme shear forces used to disperse the microcapsules in the solvent. The radical concentration is sensitive to synthesis conditions, being lower in μCaps-B-2 than μCaps-B-1. Estimates from NMR and EPR disagree significantly on the concentration of unpaired electrons μCaps-B-1. While EPR calibrated by weak pitch and nanodiamond indicates only one electron per  $(50 \text{ nm})^3$ , NMR requires about one electron per  $(5 \text{ nm})^3$  since the dipolar fields of the electrons over distances > 5 nm are too weak to significantly affect nuclear relaxation.

**Solid-state NMR in industry**. In general, the use of NMR in industry is focused almost exclusively on product development. The main workhorse is solution NMR, which is used to

elucidate the structures of new small- to medium-size molecules. Solid-state NMR is employed far less. Its uses are mainly in the pharmaceutical industry, for drug analysis in general; comparison of active pharmaceutical ingredients (APIs) in pure form and in formulation; analysis of crystalline polymorphs since these may influence the solubility and delivery of APIs; determination and quantification of amorphous phases; and studies of APIs confined in delivery systems. <sup>28,29</sup> The study of delivery systems is also of great importance for the fragrance and flavor industry, which is constantly developing modified encapsulation systems to address - among other things - biodegradability and requirements resulting from the European microplastics restriction. Unfortunately, almost no publications can be found on this topic, although solid-state NMR methods are very useful in this context, in particular for cross-linked materials. Solid-state NMR techniques including CP/MAS, <sup>13</sup>C and <sup>15</sup>N multiCP, multiplicity editing, <sup>1</sup>H inversion recovery and <sup>1</sup>H spin diffusion are therefore of high interest for the industry and have proven to be extremely useful in the development and optimization of new delivery systems, to obtain information about structure and composition, to study multiphasic systems, and to address patent and regulatory issues.

#### **Conclusions**

The structure of cross-linked multi-component polymer microcapsules and their neat precursors, in particular an amine–aldehyde resin, has been characterized by multinuclear (<sup>13</sup>C, <sup>15</sup>N, {<sup>14</sup>N}, and <sup>1</sup>H) solid-state NMR without isotopic enrichment. Overall composition information was obtained from quantitative multiCP <sup>13</sup>C NMR spectra, which documented and quantified composition variations in different batches of the microcapsules. <sup>13</sup>C NMR with C-N and CH spectral editing identified N-CH-O-C from amine—aldehyde reaction products, while dipolar dephasing revealed OCH<sub>3</sub> specifically from DME. MultiCP <sup>15</sup>N NMR spectra distinguished melamine, guanazole, tertiary/secondary/primary amines, and indirectly urea. The NMR analysis yielded enough structural detail to enable calculation of the elemental composition of Resin-9, which was consistent with combustion analysis. A new structural model provided better agreement with the quantitative and selective NMR data than previous proposals. The analysis was helped by the observation of crystals of a fairly simple tricyclic molecule in one batch of the resin. Significant changes in resin composition upon incorporation into the microcapsules were observed, such as transformation and loss of urea as well as the unexpected formation of more primary amines due to opening of ring structures in the neat resin. The amount of melamine, urea, and Alcapsol in the microcapsules was quantified in weight%. <sup>1</sup>H spin diffusion resulted in quick equilibration in <sup>1</sup>H-<sup>13</sup>C HetCor spectra and in <sup>1</sup>H inversion recovery with <sup>13</sup>C detection, proving mixing of melamine, urea, Ambergum, and Alcapsol in the microcapsules on the 4-nm scale. Uncommonly fast  $T_{1H}$  and rapid non-exponential  $T_{1C}$ 

relaxation indicated persistent radicals, confirmed by EPR. The nearly uniform non-exponential  $T_{\rm 1C}$  relaxation independently corroborated the fine mixing of all microcapsule components on the nanometer scale.

**Acknowledgments**. The authors thank Dr. Sarah Cady for the EPR measurements. The NMR spectrometer was funded by the NSF-MRI program (Award No. 1726346).

**Conflicts of Interest**. The authors declare no conflict of interest.

#### **References Cited**

- (1) Bovey, F. A.; Jelinski, L.; Mirau, P. A. *Nuclear Magnetic Resonance Spectroscopy*; 2nd ed.; Academic Press: San Diego, 1988.
- (2) Harris, R. K. *Nuclear magnetic resonance spectroscopy: a physiochemical view*; Longman Scientific and Technical: Avon, 1986.
- (3) Schmidt-Rohr, K.; Spiess, H. W. *Multidimensional Solid-State NMR and Polymers*; 1st ed.; Academic Press: London, 1994.
- (4) Mao, J.-D.; Cao, X.; Olk, D. C.; Chu, W.; Schmidt-Rohr, K. Advanced solid-state NMR spectroscopy of natural organic matter. *Prog. Nucl. Magn. Reson. Spectrosc.* **2017**, *100*, 17-100.
- (5) Ernst, R. R.; Bodenhausen, G.; Wokaun, A. *Principles of Nuclear Magnetic Resonance in One and Two Dimensions*; Clarendon Press: Oxford, 1987.
- (6) Huo, J.; Duan, P.; Pham, H. N.; Datye, A.; Schmidt-Rohr, K.; Shanks, B. H. Improved hydrothermal stability of Pd nanoparticles on nitrogen-doped carbon supports. *Catal. Sci. Technol.* **2018**, *8*, 3548-3561
- (7) Johnson, R. L.; Schmidt-Rohr, K. Quantitative solid-state <sup>13</sup>C NMR with signal enhancement by multiple cross polarization. *JMR* **2014**, *239*, 44-49.
- (8) Duan, P.; Schmidt-Rohr, K. Composite-Pulse and Partially Dipolar Dephased MultiCP for Improved Quantitative 13C Solid-State NMR. *JMR* **2017**, *285*, 68-78.
- (9) León, G.; Paret, N.; Fankhauser, P.; Grenno, D.; Erni, P.; Ouali, L.; Berthier, D. L. Formaldehyde-free melamine microcapsules as core/shell delivery systems for encapsulation of volatile active ingredients. *RSC Adv.* **2017**, *7*, 18962-18975.
- (10) Schmidt-Rohr, K.; Mao, J. D. Efficient CH-Group Selection and Identification in 13C Solid-State NMR by Dipolar DEPT and 1H Chemical-Shift Filtering. *J. Am. Chem. Soc.* **2002**, *124*, 13938-13948.
- (11) Schmidt-Rohr, K.; Mao, J. D. Selective observation of nitrogen-bonded carbons in solid-state NMR by saturation-pulse induced dipolar exchange with recoupling. *Chem. Phys. Lett.* **2002**, *359*, 403-411.
- (12) Anderson, J. M.; Johnson, R. L.; Schmidt-Rohr, K.; Shanks, B. H. Solid state NMR study of chemical structure and hydrothermal deactivation of moderate-temperature carbon materials with acidic SO<sub>3</sub>H sites. *Carbon* **2014**, *74*, 333-345.
- (13) Mao, J.-D.; Schmidt-Rohr, K. Accurate Quantification of Aromaticity and Nonprotonated Aromatic Carbon Fraction in Natural Organic Matter by <sup>13</sup>C Solid State NMR. *Environ. Sci. Technol.* **2004**, *38*, 2680-2684.
- (14) Y. Shao, L. F. M., Y. Jung, J. Kussmann, C. Ochsenfeld, S. T. Brown, A. T. B. Gilbert, L. V. Slipchenko, S. V. Levchenko, D. P. O'Neill, R. A. DiStasio Jr., R. C. Lochan, T. Wang, G. J.

- O. Beran, N. A. Besley, J. M. Herbert, C. Y. Lin, T. Van Voorhis, S. H. Chien, A. Sodt, R. P. Steele, V. A. Rassolov, P. E. Maslen, P. P. Korambath, R. D. Adamson, B. Austin, J. Baker, E. F. C. Byrd, H. Dachsel, R. J. Doerksen, A. Dreuw, B. D. Dunietz, A. D. Dutoi, T. R. Furlani, S. R. Gwaltney, A. Heyden, S. Hirata, C-P. Hsu, G. Kedziora, R. Z. Khalliulin, P. Klunzinger, A. M. Lee, M. S. Lee, W. Z. Liang, I. Lotan, N. Nair, B. Peters, E. I. Proynov, P. A. Pieniazek, Y. M. Rhee, J. Ritchie, E. Rosta, C. D. Sherrill, A. C. Simmonett, J. E. Subotnik, H. L. Woodcock III, W. Zhang, A. T. Bell, A. K. Chakraborty, D. M. Chipman, F. J. Keil, A. Warshel, W. J. Hehre, H. F. Schaefer, J. Kong, A. I. Krylov, P. M. W. Gill, M. Head-Gordon; Advances in methods and algorithms in a modern quantum chemistry program package. *Phys. Chem. Chem. Phys.* **2006**, *8*, 3172-3191.
- (15) Wavefunction, Inc. Spartan '16. Irvine, CA 2016.
- (16) Bennett, A. E.; Rienstra, C. M.; Auger, M.; Lakshmi, K. V.; Griffin, R. G. Heteronuclear Decoupling in Rotating Solids. *J. Chem. Phys.* **1995**, *103*, 6951-6958.
- (17) Hahn, E. L. Spin Echoes. Phys. Rev. 1950, 80, 580-594.
- (18) Dixon, W. T.; Schaefer, J.; Sefcik, M. D.; Stejskal, E. O.; McKay, R. A. Total suppression of sidebands in CPMAS C-13 NMR. *J. Magn. Reson.* (1969) **1982**, 49, 341-345.
- (19) Fung, B. M.; Khitrin, A. K.; Ermolaev, K. An improved broadband decoupling sequence for liquid crystals and solids. *J. Magn. Reson.* **2000**, *142*, 97-101.
- (20) Abragam, A. The Principles of Nuclear Magnetism; Oxford University Press: 1983, p 64.
- (21) Caravatti, P.; Braunschweiler, L.; Ernst, R. R. Heteronuclear correlation spectroscopy in rotating solids. *Chem. Phys. Lett.* **1983**, *100*, 305-310.
- (22) A. Bielecki; A.C. Kolbert; H.J.M. De Groot; R.G. Griffin; Levitt, M. H. In *Adv. Magn. Opt. Reson.*; Elsevier: 1990, p 111--124.
- (23) Deng, S.; Pizzi, A.; Du, G.; Lagel, M. C.; Delmotte, L.; Abdalla, S. Synthesis, structure characterization and application of melamine–glyoxal adhesive resins. *Eur. J. Wood Wood Prod.* **2017**, *76*, 283-296.
- (24) Fang, X. W.; Mao, J. D.; Levin, E. M.; Schmidt-Rohr, K. Nonaromatic core-shell structure of nanodiamond from solid-state NMR. *J. Am. Chem. Soc.* **2009**, *131*, 1426-1435.
- (25) Fritzsching, K. J.; Duan, P.; Erik, M. A.; Tibabuzo Perdomo, A. M.; Kenny, P.; Wilker, J. J.; Schmidt-Rohr, K. A Silk-like Protein with Organic Radicals Identified in Oyster Adhesive by Solid-State NMR. *ACS Appl. Bio Mater.* **2019**, *2*, 2840-2852
- (26) Chen, Q.; Schmidt-Rohr, K. Measurement of the Local <sup>1</sup>H Spin Diffusion Coefficient in Homogeneous Polymers. *Solid State NMR* **2006**, *29*, 142-152.
- (27) Clauss, J.; Schmidt-Rohr, K.; Spiess, H. W. Determination of Domain Sizes in Polymers. *Acta Polymer.* **1993**, *44*, 1-17.

- (28) Paradowska, K.; Wawer, I. Solid-state NMR in the analysis of drugs and naturally occurring materials. J. Pharm. Biomed. Analysis **2014**, *93*, 27-42.
- (29) Vogt, F. G. Solid-state NMR in drug discovery and development; *New Developments in NMR*, 2 (New Applications of NMR in Drug Discovery and Development), 43-100. Editors: Garrido, L; Beckmann, N., Royal Society of Chemistry, UK, 2013.

# **Figures with Captions**

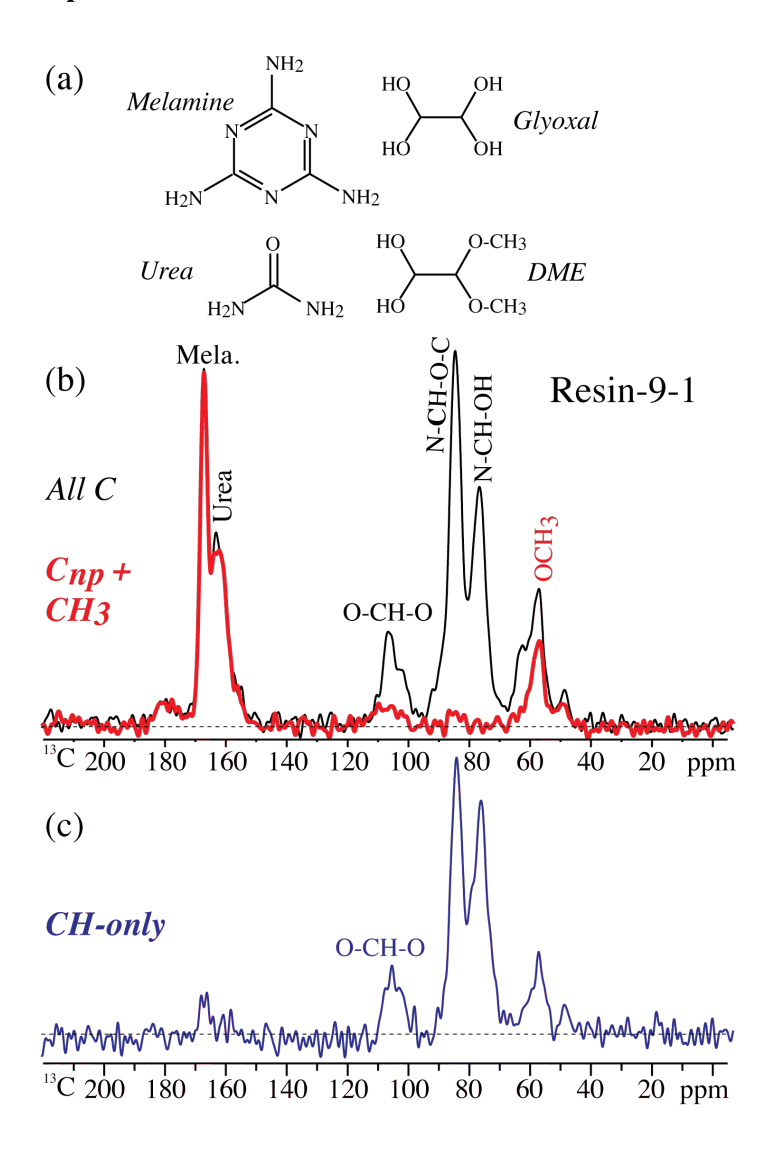


**Figure 1**. Analysis of Resin-9-1 by <sup>13</sup>C NMR with spectral editing. (a) Chemical structures of the reactants. The aldehydes are shown in their hydrated forms in water. (b) Nearly quantitative <sup>13</sup>C spectrum (thin black trace). Due to concerns about sample flowing under MAS, the spinning frequency was limited to 5.8 kHz, which reduced the sp<sup>2</sup>-C signals by 16%. Thick red trace:

signal after dipolar dephasing of non-protonated C and mobile segments, in particular rotating CH<sub>3</sub> groups. (c) CH-only spectrum from dipolar DEPT.<sup>10</sup>

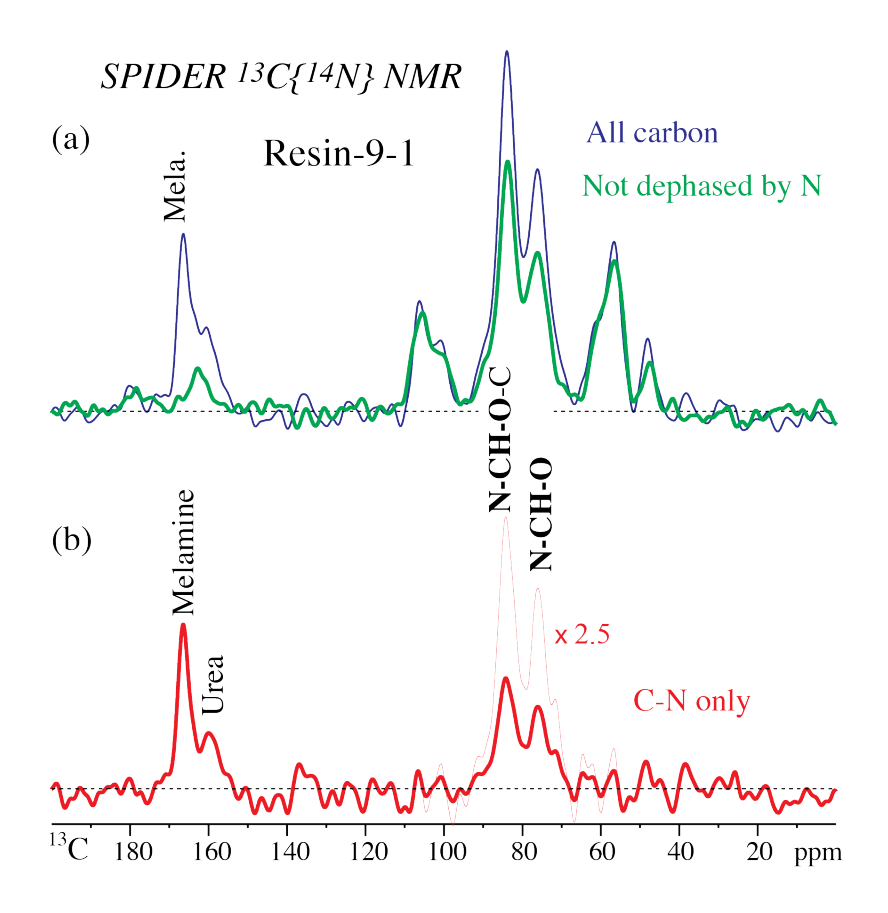


**Figure 2**. Detection of C bonded to N in Resin-9-1 by SPIDER  $^{13}$ C $\{^{14}$ N $\}$  NMR at 5 kHz MAS. (a) Full spectrum  $S_0$  (thin blue top trace) without  $^{14}$ N irradiation and spectrum  $S_0$  after  $^{13}$ C $^{-14}$ N recoupling (thicker green lower trace). (b) Difference spectrum  $\Delta S = S_0 - S$  of C bonded to N. Thin dashed line: signal at < 100 ppm scaled up by a factor of 2.5.

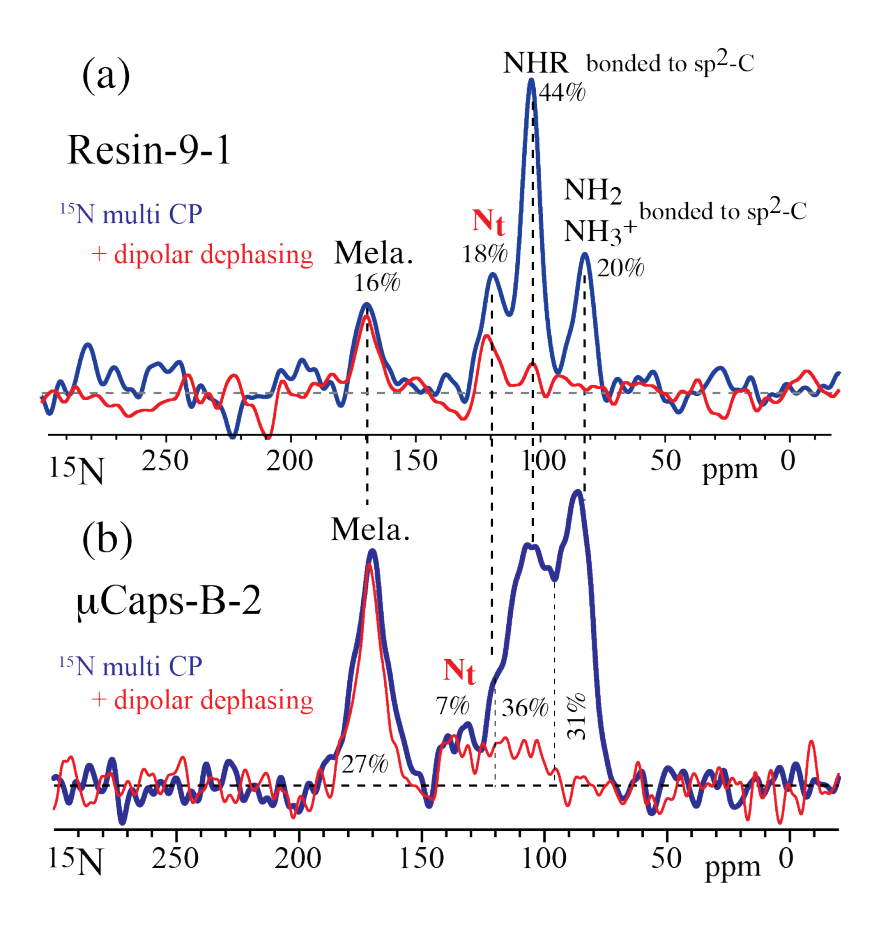


**Figure 3**. MultiCP <sup>15</sup>N NMR of (a) Resin-9-1 and (b)  $\mu$ Caps-B-2. Thick blue trace: Full spectrum; thin red trace: after dipolar dephasing by gated decoupling for 2  $t_r$ .

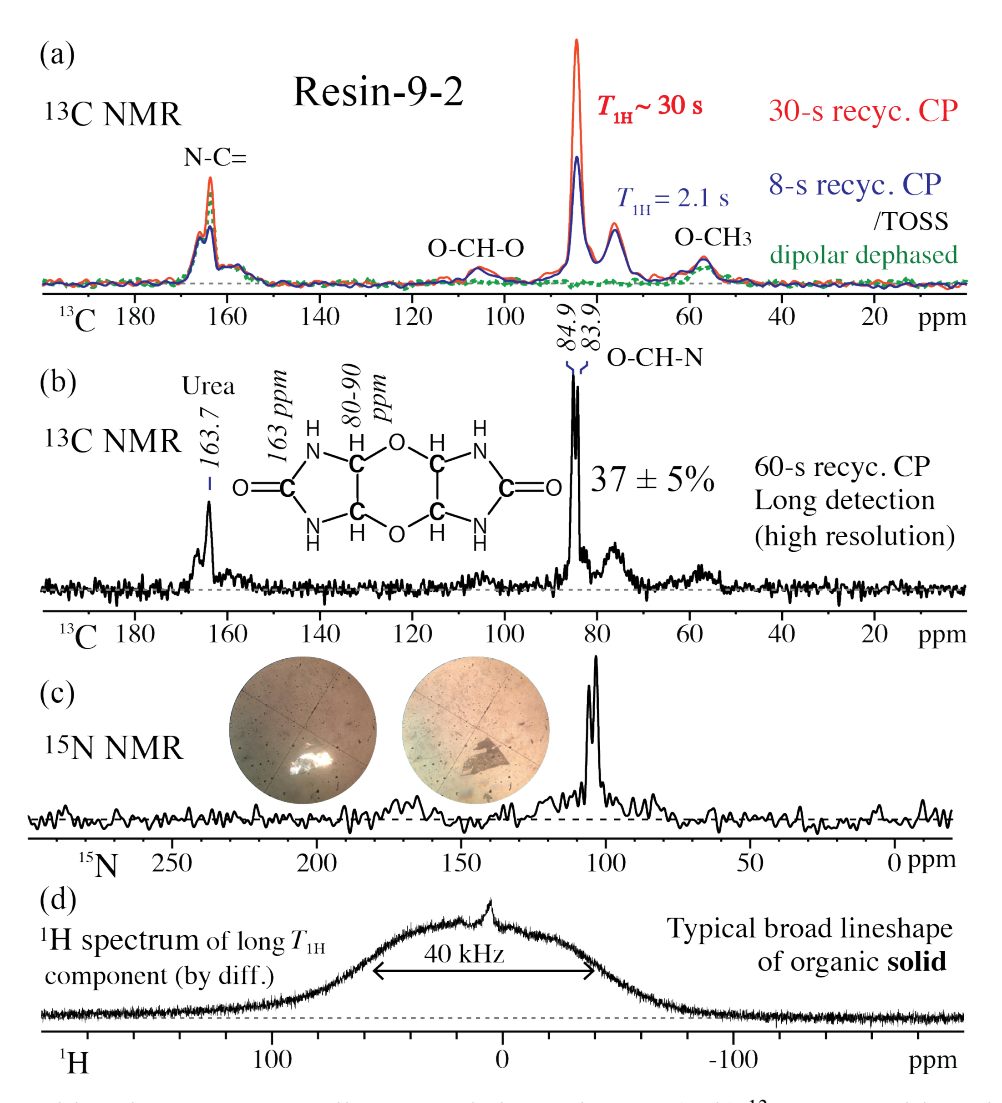


**Figure 4.** Multinuclear NMR revealing crystals in Resin-9-2. (a, b)  $^{13}$ C NMR with various recycle delays and resolution settings; (c)  $^{15}$ N NMR; (d)  $^{1}$ H NMR of the slowly-relaxing components, with the short- $T_{1H}$  components observed after an 8-s recycle delay subtracted out. The circular insets in c) show images of this sample in a polarized-light microscope for two different polarizer orientations, revealing birefringent crystals (field of view: 0.22 mm across).

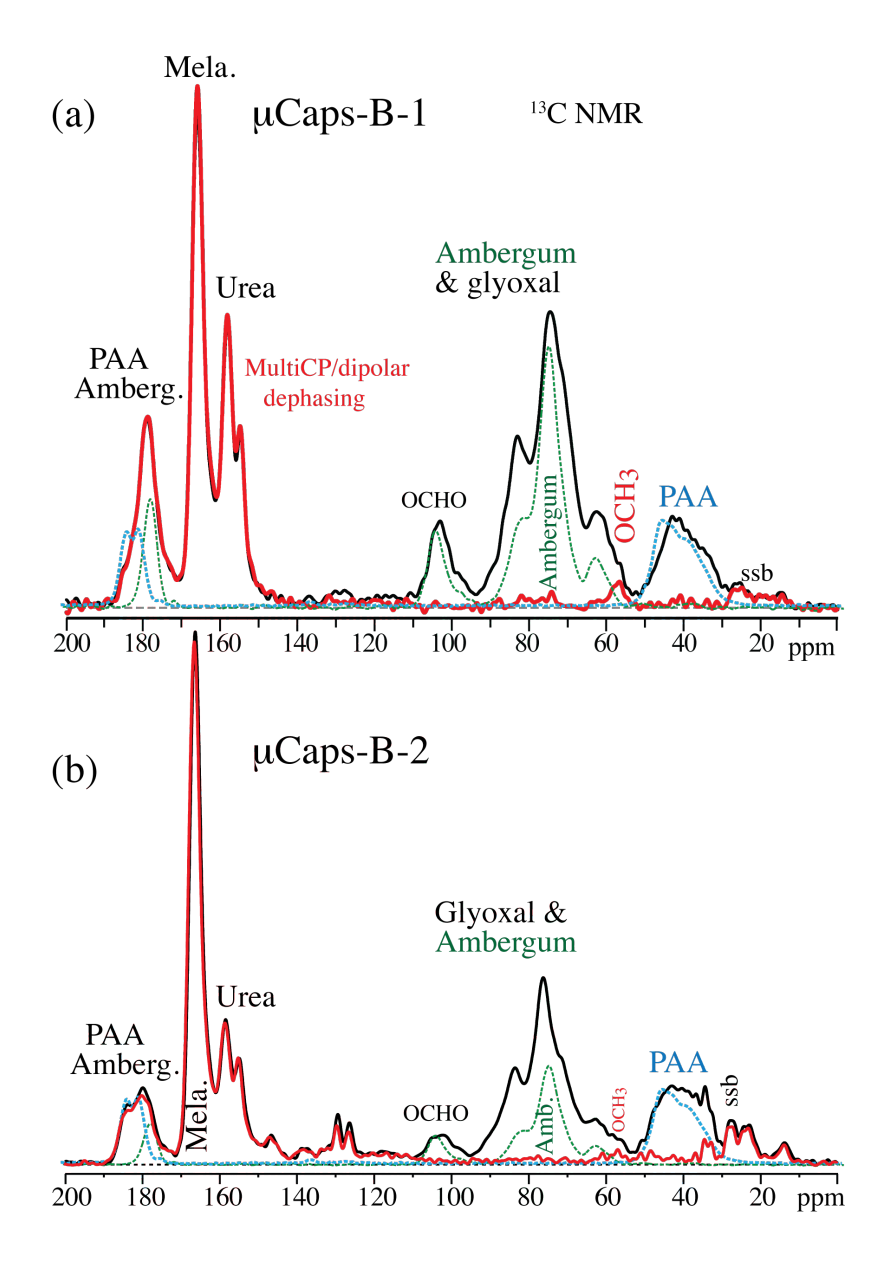


**Figure 5**. Comparison of different batches of  $\mu$ Caps-B by  $^{13}$ C NMR. (a)  $\mu$ Caps-B-1; (b)  $\mu$ Caps-B-2. Black line: full multiCP spectra; red line: after recoupled dipolar dephasing. Spectra of Ambergum (dashed green) and Alcapsol (PAA, dashed blue) are shown scaled for reference. "ssb": spinning sideband.

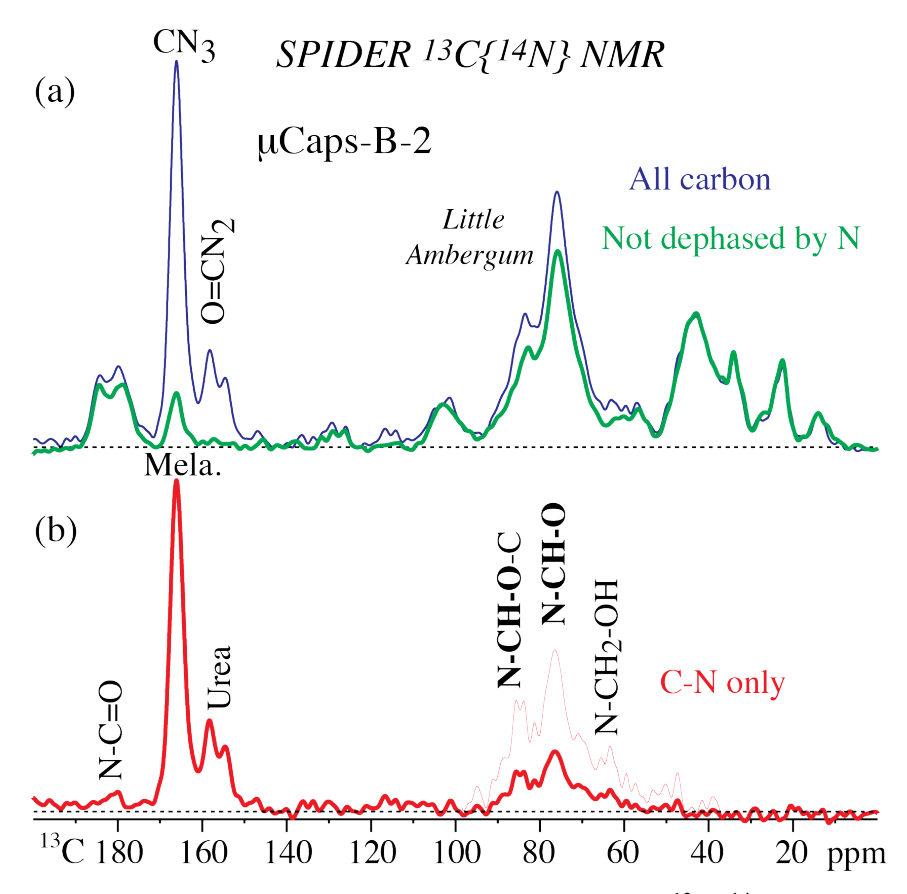


**Figure 6**. Detection of C bonded to N in  $\mu$ Caps-B-2 by SPIDER <sup>13</sup>C{<sup>14</sup>N} NMR at 5 kHz MAS. (a) Thin blue line: Spectrum without <sup>14</sup>N dipolar recoupling ( $S_0$ ). Thick green line: Spectrum with <sup>14</sup>N dipolar recoupling ( $S_0$ ). (b) Difference spectra  $\Delta S = S_0 - S$  of C bonded to N. Thin dashed line: signal at < 100 ppm scaled up by a factor of 2.5.

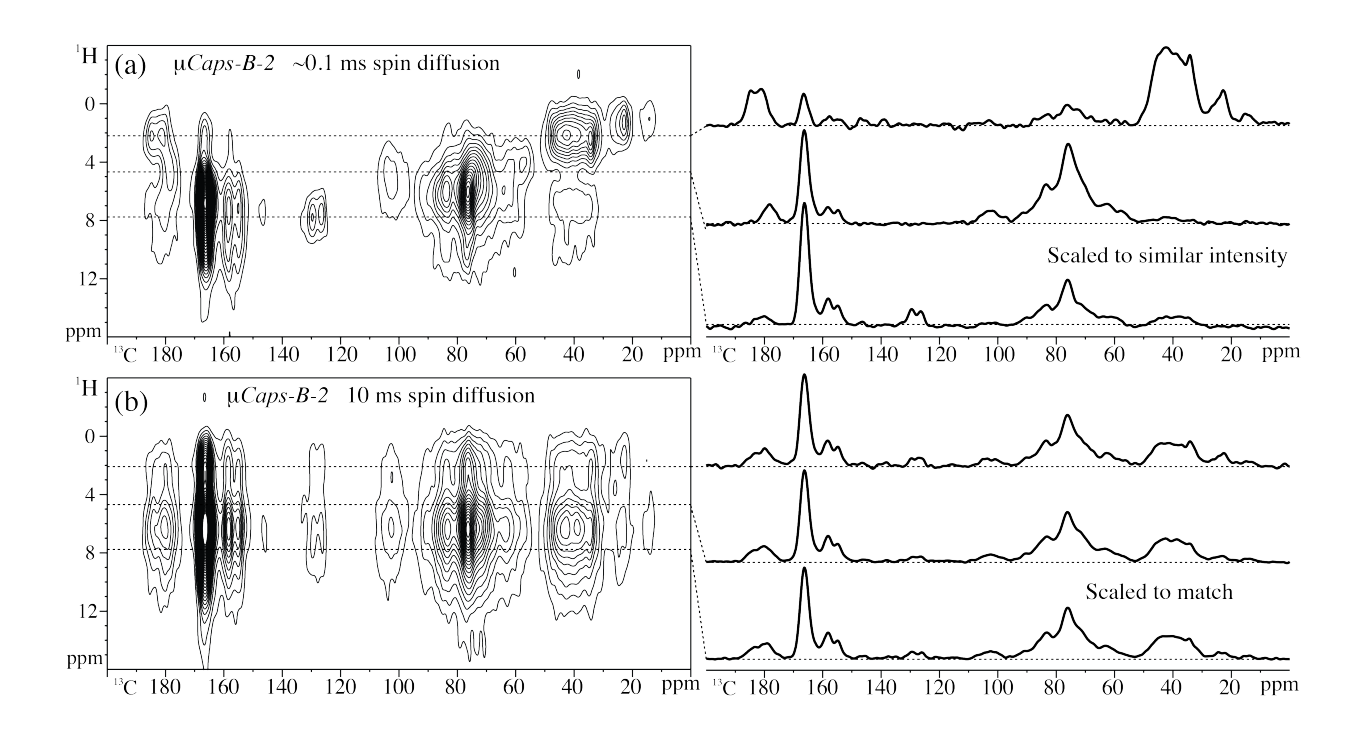


**Figure 7**.  $^{1}\text{H-}^{13}\text{C}$  HetCor NMR spectra detecting component mixing in  $\mu\text{Caps-B-2}$ . (a) Local spin diffusion during CP of 0.5 ms duration; (b) 10-ms spin diffusion equilibrating the magnetization, characterized by matching horizontal cross sections.

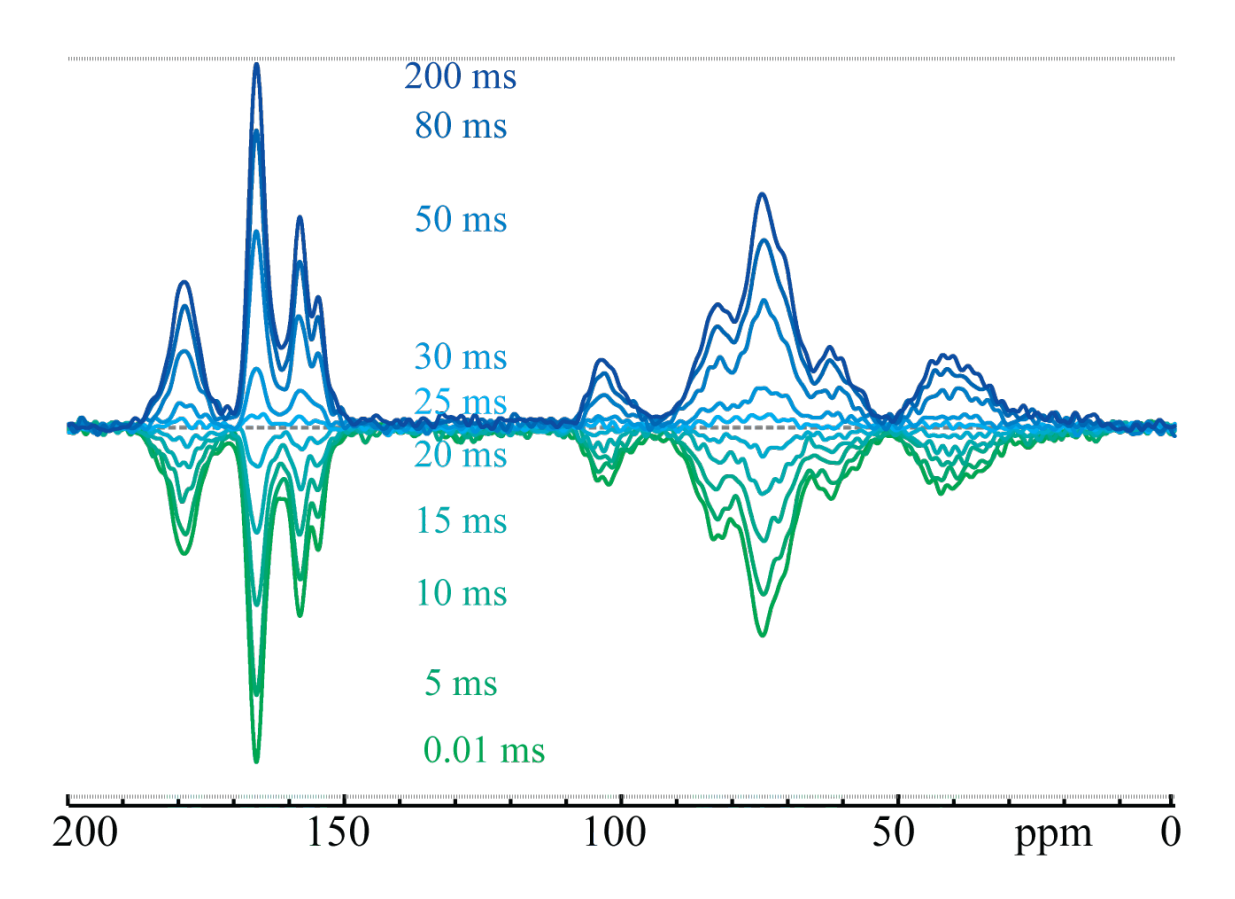


**Figure 8.** Series of  ${}^{13}\text{C}$  spectra of  $\mu\text{Caps-B-1}$  after  ${}^{1}\text{H}$  inversion recovery for the indicated times, recorded at 14 kHz MAS. A simultaneous zero crossing of all components is observed near 25 ms of inversion recovery.

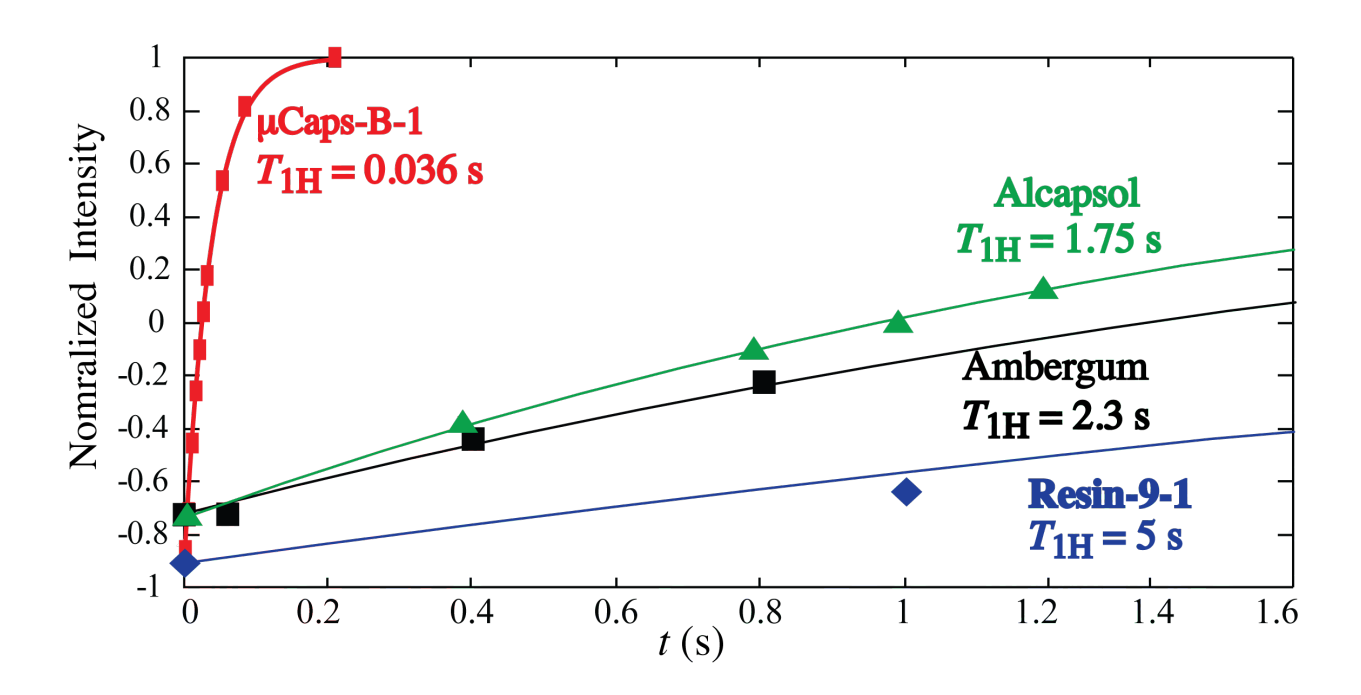


**Figure 9.**  $^{1}$ H inversion recovery ( $^{13}$ C-detected intensity as a function of recovery time) of  $\mu$ Caps-B-1, compared with that of its neat ingredients Resin-9, Ambergum, and Alcapsol (PAA).

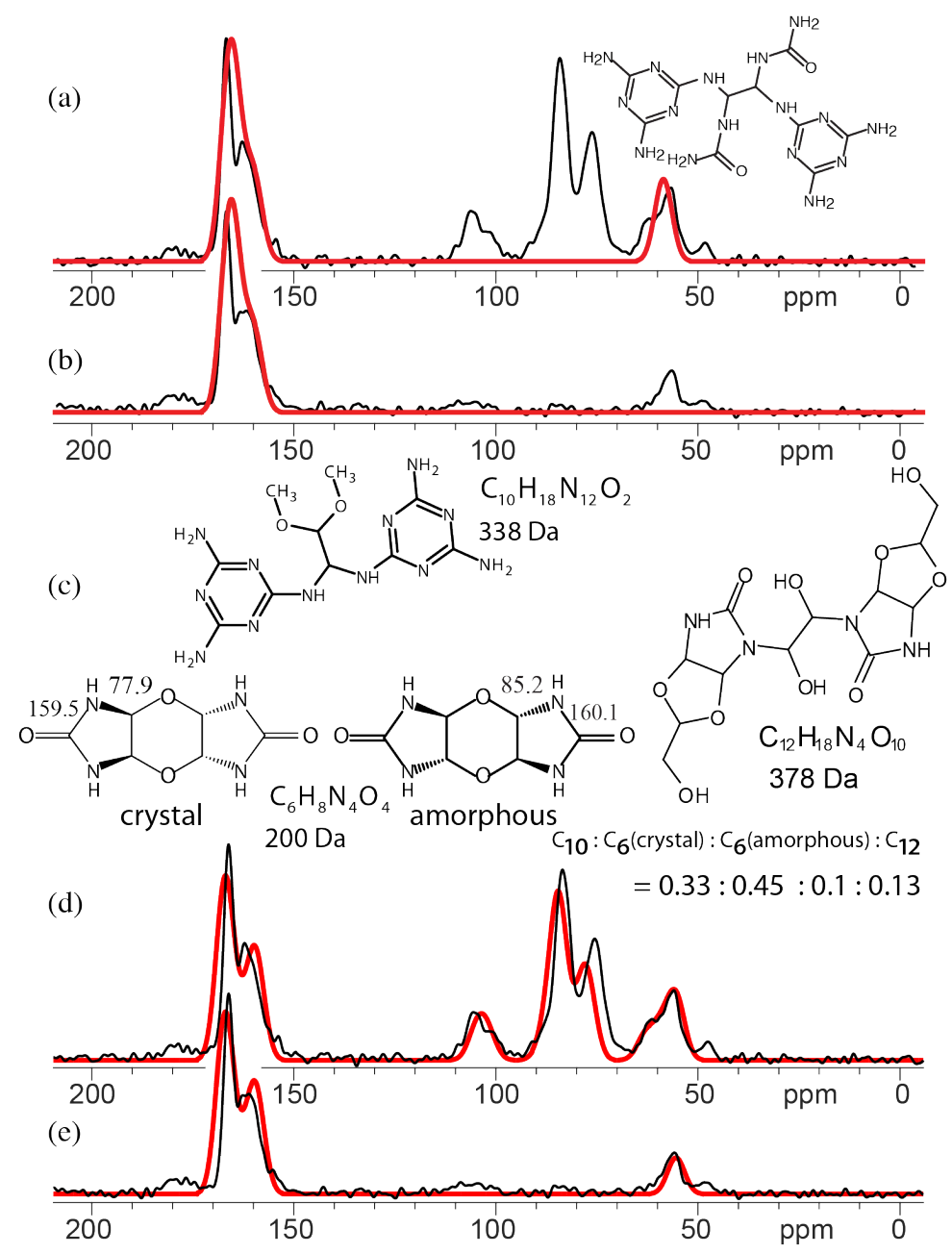


**Figure 10**. Structural analysis of Resin-9-1. (a) Structural model of 'oligomer 9a' in ref.<sup>9</sup> and corresponding predicted spectrum (thick red line), compared with the experimental spectrum (thin black line), with the intensity of the sp<sup>2</sup>-hybridized carbons scaled up by 19% to correct for effects of relatively slow 5.8-kHz magic-angle spinning; (b) spectrum after dipolar dephasing. (c) Four-component structural model and (d) corresponding simulated full spectrum (thick red line); (e) spectrum after dipolar dephasing.

**Figure 11.** Diastereomers with relative configurations and quantum-chemically predicted <sup>13</sup>C NMR chemical shifts (in ppm) of the crystalline tricyclic compound in Resin-9-2.